AGU PUBLICATIONS

JGR

Journal of Geophysical Research: Atmospheres

RESEARCH ARTICLE
10.1002/2013JD020872

Key Points:
- First time ground retrievals of cloud properties in tropical rain shadow region
- Less probability of occurrence of higher R_e
- Biases between ground and MODIS cloud products are more over tropical region

Supporting Information:
- Readme
- Figure S1

Correspondence to:
B. Padmakumari,
padma@tropmet.res.in

Citation:
Harikishan, G., B. Padmakumari, R. S. Maheskumar, G. Pandithurai, and Q. L. Min (2014), Macrophysical and microphysical properties of monsoon clouds over a rain shadow region in India from ground-based radiometric measurements, *J. Geophys. Res. Atmos.*, *119*, doi:10.1002/2013JD020872.

Received 10 SEP 2013
Accepted 25 MAR 2014
Accepted article online 30 MAR 2014

Macrophysical and microphysical properties of monsoon clouds over a rain shadow region in India from ground-based radiometric measurements

G. Harikishan[1], B. Padmakumari[1], R. S. Maheskumar[1], G. Pandithurai[1], and Q. L. Min[2]

[1]Indian Institute of Tropical Meteorology, Pune, India, [2]Atmospheric Sciences Research Center, New York, USA

Abstract The important radiative properties of clouds such as cloud optical depth (COD) and droplet effective radii (R_e) are retrieved from the simultaneous measurements by ground-based multifilter rotating shadowband radiometer (MFRSR) and microwave radiometric profiler (MWRP), colocated at Mahabubnagar, a rain shadow region in southern Indian peninsula. Min and Harisson's (1996) retrieval algorithm is used for the first time to derive monsoon cloud properties in India. COD and liquid water path (LWP) retrieved from two independent instruments of MFRSR and MWRP showed reasonably good correlation. During monsoon (July to September) and postmonsoon (October) months, the maximum probability of occurrence of COD for overcast sky is 20. The maximum probability of occurrence of LWP is 100 gm^{-2} for water clouds during monsoon months, while October showed maximum occurrence at a lower value of 50 gm^{-2}, where most of the times the cloud bases are above freezing level indicating mixed phase clouds. Maximum R_e varied from 14–16 μm (10–12%) to 12 μm (9%) during monsoon to postmonsoon transition with very less probability of occurrence indicating the characteristic feature of this region. A case study showed that the mean R_e from ground-based and aircraft measurements are 12.0 ± 3.7 μm and 8.14 ± 1.4 μm, respectively, indicating a fairly good agreement within the experimental constraints. Intercomparison of ground-based and Moderate Resolution Imaging Spectroradiometer (MODIS)-Terra and MODIS-Aqua-derived COD, LWP and R_e over the observational site for overcast and warm clouds indicates that on an average, MODIS-retrieved mean COD and LWP are underestimated, while mean R_e is overestimated as compared to ground retrievals.

1. Introduction

Clouds are the dominant modulators of the Earth's radiation budget because of their scattering and absorption of solar and infrared radiation. Small changes in their properties will alter radiation budget much more than greenhouse gases and aerosols [*Norris and Wild,* 2007]. Over the Indian subcontinent, it was observed that the rate of solar dimming is twice as large during cloudy days as compared to clear-sky days [*Padma Kumari and Goswami*, 2010]. The variability in incoming radiation is largely dependent on cloud thickness, cloud base height, horizontal extent, and microphysical characteristics. It is challenging to retrieve cloud properties because of their high variability in time and space. Efforts have been made to retrieve cloud properties from in situ, satellite, and ground-based observations. Cloud microphysical and macrophysical properties were studied with aircraft [*Slingo et al.,* 1982; *Brenguier et al.*, 2000; *Pawlowska et al.,* 2006; *Morwal et al.*, 2012; *Pandithurai et al.*, 2012; *Konwar et al.*, 2012] and satellite measurements [*Roebeling et al.*, 2006; *Kubar et al.*, 2009; *Christensen and Stephens,* 2011; *Min et al.,* 2012], while ground-based retrievals are limited. Retrieval of cloud microphysical properties from satellite measurements still has large uncertainties, and most of the retrieval algorithms for satellite measurements were first tested with ground-based remote sensing measurements. From the ground-based remote sensing, retrieval algorithms have been developed to infer COD, which is vital for any cloud-radiation parameterization, using direct and diffuse radiation measurements from a broadband radiometer such as pyranometer [*Leontieva and Stamnes*, 1996; *Dong et al.*, 1997; *Barker et al.*, 1998] and also from a narrow band radiometer such as MFRSR for overcast cloudy conditions [*Min and Harrison*, 1996a; *Min et al.*, 2004a; *Wang and Min*, 2008; *Madhavan et al.*, 2012]. Cloud droplet effective radii R_e, which is one of the most fundamental cloud properties for understanding aerosol-cloud interactions, is also retrieved from the combined ground-based shortwave flux and microwave radiometer observations [*Min and Harrison*, 1996a; *Kim et al.*, 2003; *Min and Duan*, 2005; *Feingold et al.*, 2006].

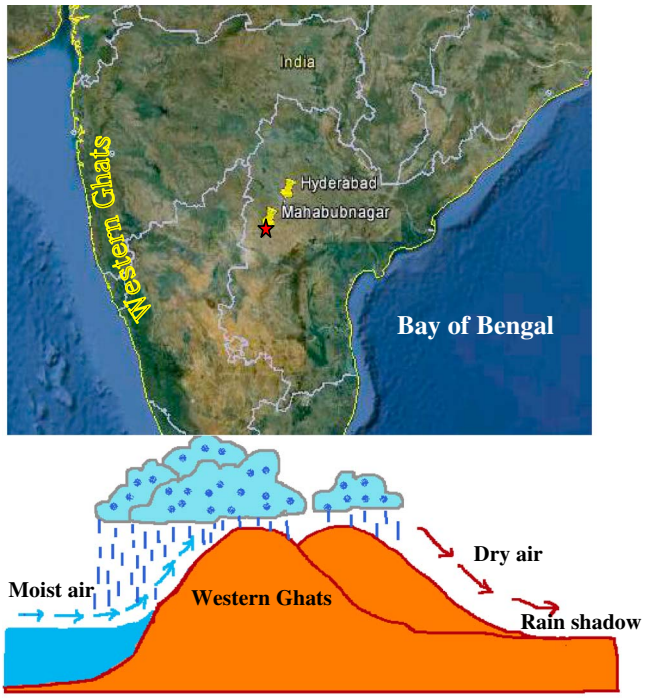

Figure 1. Map of southern India showing the observational location Mahabubnagar, which is 100 km to the south west of Hyderabad. Below figure represents a schematic showing the rainfall pattern along west coast.

Some other retrieval methods are based on cloud radar and microwave radiometer measurements [*Liao and Sassen,* 1994; *Wang et al.*, 2004] and also from single instruments using zenith radiance measured at visible and near-infrared wavelengths [*Kikuchi et al.*, 2006; *McBride et al.*, 2011; *Chiu et al.*, 2012]. However, due to high spatial and temporal variability of clouds, it is challenging to retrieve cloud properties accurately.

India is mostly dependent on south west monsoon which occurs during June to September and accounts for over 70% of rainfall in the country [*Rao,* 1976]. Apart from large-scale monsoon circulation, local convective activities also contribute in the formation of clouds and precipitation during the monsoon season. Atmospheric aerosols play an important role in modulating the cloud macrophysical and microphysical properties and thereby precipitation in the monsoon environment. To understand aerosol-cloud interactions during south west monsoon, a national experiment called CAIPEEX (Cloud Aerosol Interaction and Precipitation Enhancement Experiment) was conducted with an instrumented aircraft from 2009 to 2011 (http://www.tropmet.res.in/~caipeex/). Ground-based observations of cloud properties over the Indian monsoon region do not exist. This study presents for the first time the ground-based retrievals of cloud optical properties such as COD, LWP, and R_e over a rain shadow region.

2. Area of Observations

Over a large part of the Indian subcontinent, most of the rainfall occurs in the months of June to September during the summer monsoon. July and August are the peak monsoon months, and monsoon withdrawal starts in September. It is well known that the monsoon rainfall is dependent on the position and intensity of the monsoon trough formed in the northern India [*Rao*, 1976]. When the axis of the trough moves north of its normal position and lies close to the foot hills of the Himalayas, rainfall weakens over most of the plains of northern India (a condition characteristic of the so-called "break" in the monsoon). Another feature of a "break" is the westward passage of low-pressure systems across the Indian peninsula. Parts of the peninsula, which lie in the rain shadow of the Western Ghats, obtain much of their monsoon rainfall during break situations [*Das*, 1995]. When the trough moves to the south of its normal position, the monsoon becomes active.

The instruments multifilter rotating shadowband radiometer (MFRSR) and microwave radiometric profiler (MWRP) were operated simultaneously during the Integrated Ground Observational Campaign (IGOC), which was conducted at Mahabubnagar (16°46′N and 77°56′E; 440 m above mean sea level (AMSL)) in southern India from July to October 2011. Mahabubnagar is a town situated 100 km to the southwest of a highly populated and polluted city, Hyderabad, in the southern peninsula (Figure 1). This location is situated to the east of the leeward side of the Western Ghats and falls under rain shadow region which is mostly drought prone area. Precipitable water content (PWC) and winds obtained from NCEP reanalysis data at 850 hPa for the monsoon months July–September and postmonsoon month October 2011 are shown in Figure 2.

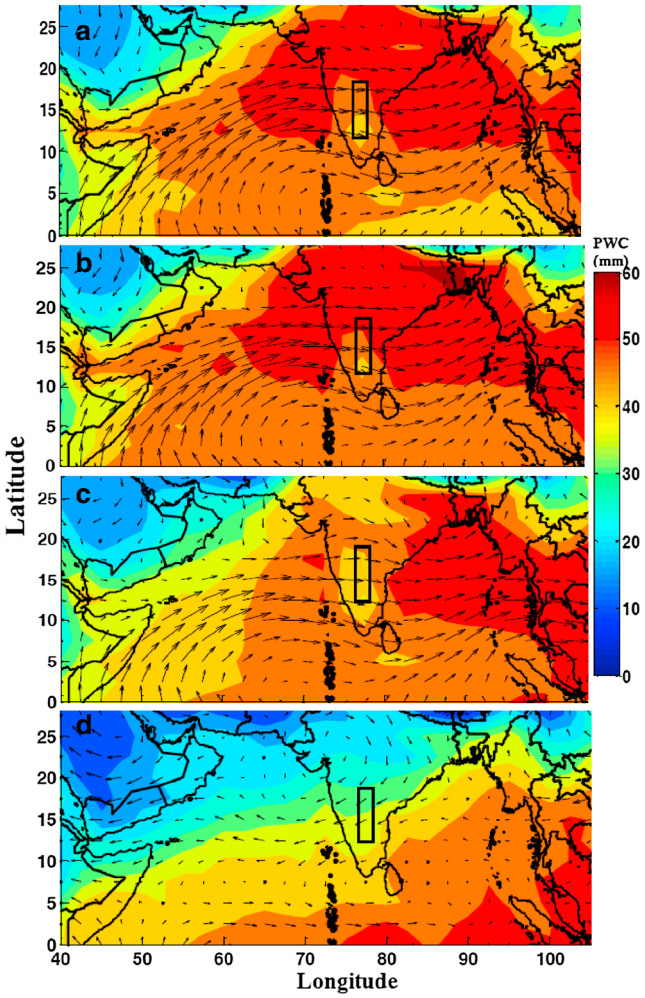

Figure 2. Precipitable water content (PWC) and surface winds at 850 hPa obtained from NCEP reanalysis data for the months (a) July, (b) August, (c) September, and (d) October. Color bar represents PWC in millimeter; the rectangle in each figure represents the rain shadow region.

All the months showed less PWC over the rain shadow region (marked by a box) as compared to west coast of India, and among the four months, August showed more PWC over the rain shadow region. The subdivisions to the leeward side of the Western Ghats receive rainfall of about 20% of that over the windward side, and this known feature of steep decrease in the rainfall over the lee side of the Ghats is unique and not found elsewhere in India [*Rao*, 1976]. Clouds in the rain shadow region are mostly nonprecipitating in nature and are influenced by the underlying polluted aerosols [*Konwar et al.*, 2010]. Hence, this region is highly suitable for the ground-based retrievals of cloud properties, and the measurements reported over this region are first of its kind.

3. Data and Methodology

3.1. Ground-Based Instrumentation

The radiometers MFRSR and MWRP were operated continuously over the region at a high temporal resolution of 1 min. MFRSR is a seven-channel pyranometer with a hemispheric field of view and a rotating shadowband. It measures irradiances at six narrow spectral bands centered at 415, 500, 615, 673, 870, and 940 nm and at one broadband (0.3–1.1 μm). The basic outputs are direct normal, diffuse horizontal, and total horizontal solar irradiances collected under different sky conditions [*Harrison and Michalsky*, 1994]. Among various measurement techniques for surface radiation, shadowband technique has proven robust for its accurate determination of atmospheric transmittances without requiring absolute calibration for long term deployment [*Harrison et al.*, 1994].

The MWRP (MP-3000A) provided the profiles of temperature, humidity, and cloud liquid water content as a function of height or pressure by measuring microwave radiance or brightness temperature at 21 frequencies near the water vapor resonance centered at 22.235 GHz and 14 frequencies in the band of oxygen resonances between 51 and 59 GHz and works for almost all weather conditions [*Liljegren et al.*, 2001]. The beam width varies from 6.1° at 22 GHz to 2.2° at 59 GHz. The cloud base height (CBH) was estimated from a zenith-pointing infrared radiometer mounted in MWRP which measures downwelling infrared radiation (IR) in the 9.6–11.5 μm band which is converted into cloud base temperature and in turn CBH estimates. The accuracy of IR temperature measurements is $0.5 + 0.007\ \Delta T$ °C where $\Delta T = T_{ambient} - T_{cloud}$. As CBH is a derived parameter from cloud base temperature, the uncertainty can be ± 200 m. In the data, rain contamination is identified by a flag that is activated when the rain sensor mounted on the radiometer detects water drops. The typical uncertainty in the retrievals of LWP is ~20 gm^{-2} for LWP $< 200\ gm^{-2}$ and ~10% for LWP $> 200\ gm^{-2}$ [*Dong et al.*, 2000; *Liljegren et al.*, 2001]. However, the unaccounted biases in the LWP retrievals would affect the estimation of R_e. To evaluate the presence of

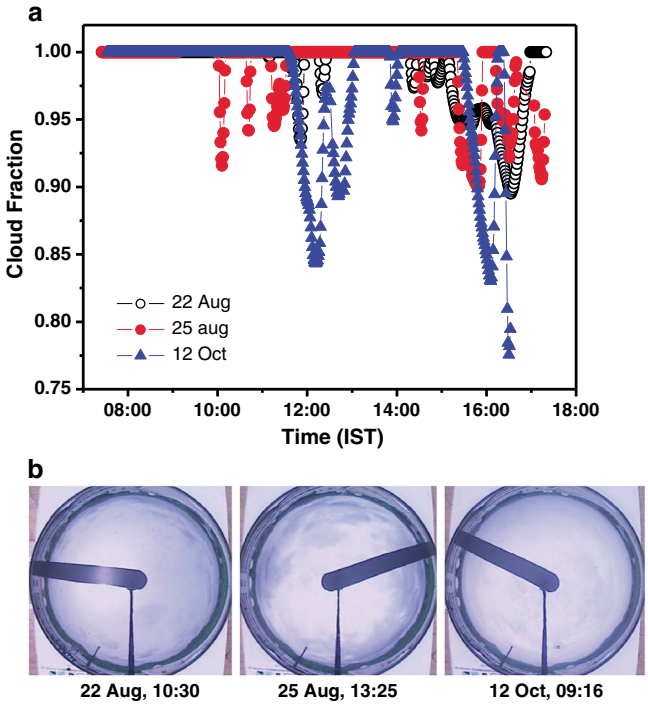

Figure 3. (a) Time series of cloud fraction and (b) sky images on different days at different timings to show the cloud coverage over the observational site.

biases, LWP distribution under clear-sky conditions [*Min et al.*, 2003; *Liu et al.*, 2013] was plotted and the observed mean is 4.9 gm^{-2} with a standard deviation of 7.6 gm^{-2}. This confirms that there were no appreciable biases in the retrievals. In the present analysis, LWP values less than 20 gm^{-2} and during rain ($>$ 700 gm^{-2}) are discarded.

Total Sky Imager (TSI) was also operated at the same location, which gives the hemispheric day time sky image at every 1 min time interval. Sky images were browsed to identify the sky conditions during the analysis of cloud properties.

3.2. Airborne, Satellite, and Other Data Sets

CAIPEEX was conducted using a research aircraft from the base Hyderabad toward the southwestern sector from the middle of September to the first week of November 2011 (http://www.tropmet.res.in/~caipeex/). The aircraft was equipped with standard instrumentations for state parameters (such as temperature, pressure, humidity, and winds), aerosol, and clouds. Forward Scattering Spectrometer Probe (FSSP) was used for cloud droplet size distribution in the size range of 3–47 μm. Cloud droplet effective radius (R_e) is derived from FSSP drop size distribution [*Stephens,* 1978b]. Data were collected at an interval of 1 s (~100 m). More details about the experiment and the instrumentation are given in *Kulkarni et al.* [2012].

Terra and Aqua Moderate Resolution Imaging Spectroradiometer (MODIS) level 2 data sets at 1 km resolution are also utilized. From MODIS level 2 cloud products, data are processed using two flag information such as cloud_Phase_Optical Properties and Cloud_Multilayer to segregate single-layer warm clouds at each pixel [*Menzel and Frey*, 2013]. PWC and wind data at 850 hPa are obtained from National Center for Environmental Prediction–National Center for Atmospheric Research (NCEP-NCAR) reanalyses [*Kalnay et al.*, 1996].

4. Retrieval Technique

In the present study, COD is retrieved from the surface measurements of narrowband spectral irradiance obtained from MFRSR, by using an iterative algorithm developed by *Min and Harrison* [1996a, 1996b], in which a radiative transfer model based on discrete ordinate radiative transfer is incorporated. The discrete ordinate model [*Stamnes et al.*, 1988] includes all orders of multiple scattering and is valid for vertically inhomogeneous, nonisothermal, and plane-parallel media. As COD is a measure of the attenuation of light passing through the atmosphere due to scattering and absorption by cloud droplets, it is derived using the observed atmospheric transmittance (rather than irradiance) and surface albedo for solar zenith angles less than 75°. Both the quantities are accurately obtained from MFRSR, as it measures both total horizontal and direct normal irradiance using the same detector by a shadowband technique. The instrument's response to the top of the atmosphere (TOA), obtained by extrapolating the Langley regression of the direct normal irradiance under clear-sky conditions, can be applied to the total horizontal irradiance. Transmittance under both clear-sky or cloudy conditions is evaluated as the ratio of measured signal at the surface to the extrapolated TOA value, which is insensitive to the absolute calibration of MFRSR. Surface albedo is obtained from the ratio of direct to diffuse irradiances on cloud free days. The wavelength of 415 nm is chosen for cloud retrievals, to avoid gaseous absorption and to have small surface albedo. COD is retrieved by a nonlinear least square method described by *Bevington* [1969].

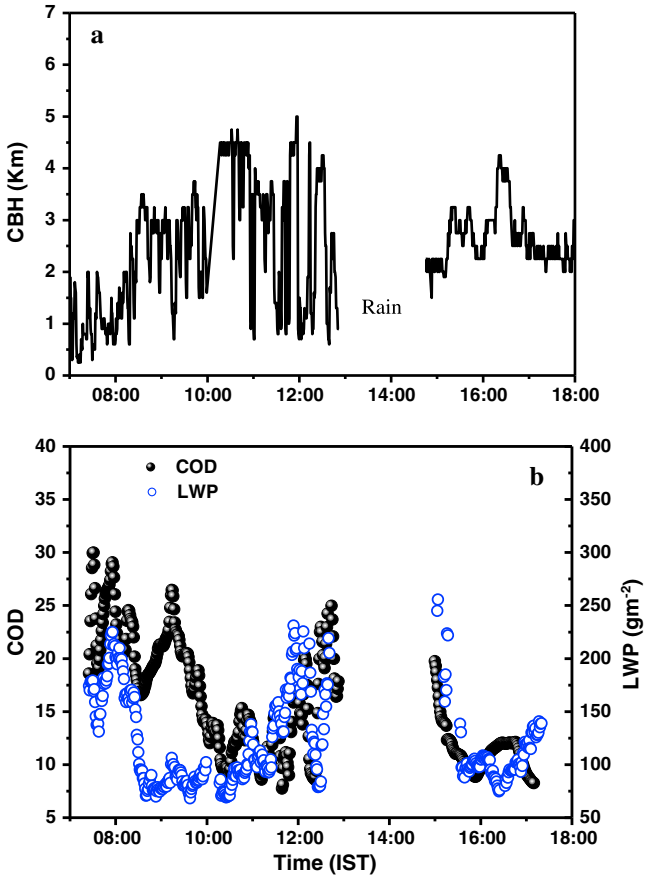

Figure 4. Time series of (a) cloud base height (CBH) and (b) cloud optical depth (COD) and liquid water path (LWP) for 22 August 2011.

Several retrieval algorithms have been developed to infer optical depths for different cloud types from MFRSR measurements. Measurements of transmission of diffuse solar radiation, in case of thick clouds [*Min and Harrison*, 1996a], and transmission of direct solar radiation, in case of thin clouds [*Min et al.*, 2004a, 2004b], were used to retrieve COD. These retrieval algorithms, which were used in the present study, were extensively tested and validated with in situ measurements [*Min et al.*, 2003, 2004a]. The uncertainty in the retrieved COD comes from the uncertainties in zenith radiance measurements and surface albedo. A 5% uncertainty in zenith radiance measurements would result in 6.7% error in COD retrievals [*Harrison and Michalsky*, 1994]. Similarly 0.5% (50%) uncertainty in surface albedo (aerosol loading) would result in 3.6% (0.5%) error in COD retrievals [*Min and Harrison,* 1996a, 1996b]. Cloud fraction is also derived from this code using transmittance ratio at two selected wavelengths 415 nm and 870 nm (procedure described in *Min et al.* [2008]), and the uncertainty observed is less than 10%. In the statistical analysis, only overcast period is considered which is defined as COD >5 for at least 1 h [*Liu et al.*, 2013] and cloud fraction equal to one.

The retrieval algorithm also uses LWP measured by MWRP to obtain R_e of the cloud droplets. R_e is estimated from COD and LWP as

$$R_e = (3*\mathrm{LWP})/(2*\mathrm{COD}*\rho_w)$$

where ρ_w represents density of water [*Stephens,* 1978a]. R_e obtained by this method represents the vertically integrated quantity governing the radiative transfer of the cloud, as both COD from MFRSR and LWP from MWRP come from vertically integrated retrievals [*Min et al.*, 2003; *Kim et al.*, 2003]. Any error in the derivation of R_e may come mostly due to the biases and errors that may arise in the measurements of LWP, especially at small optical depths and at low LWPs [*Min et al.*, 2003]. R_e retrieved by this inversion algorithm was also validated with in situ aircraft measurements during the Atmospheric Radiation Measurement (ARM) field campaign at South Great Plains site [*Min et al.*, 2003]. In the analysis, $R_e > 20\ \mu m$ is not considered, as the high values might correspond to conditions with possible light drizzle; the other possibility could be due to enhanced transmittance, which could occur due to three-dimensional effects in non-plane-parallel conditions, thus leading to an overestimation of the retrieved R_e [*Matamoros et al.*, 2011].

5. Results and Discussion

5.1. Case Studies

Investigations of few case studies on 22 August, 25 August, and 12 October 2011 are presented in this section. These cases represent different cloud types and their variability with time over the observational region. Figure 3 shows the temporal variability of cloud fraction for the above 3 days, estimated from the broadband

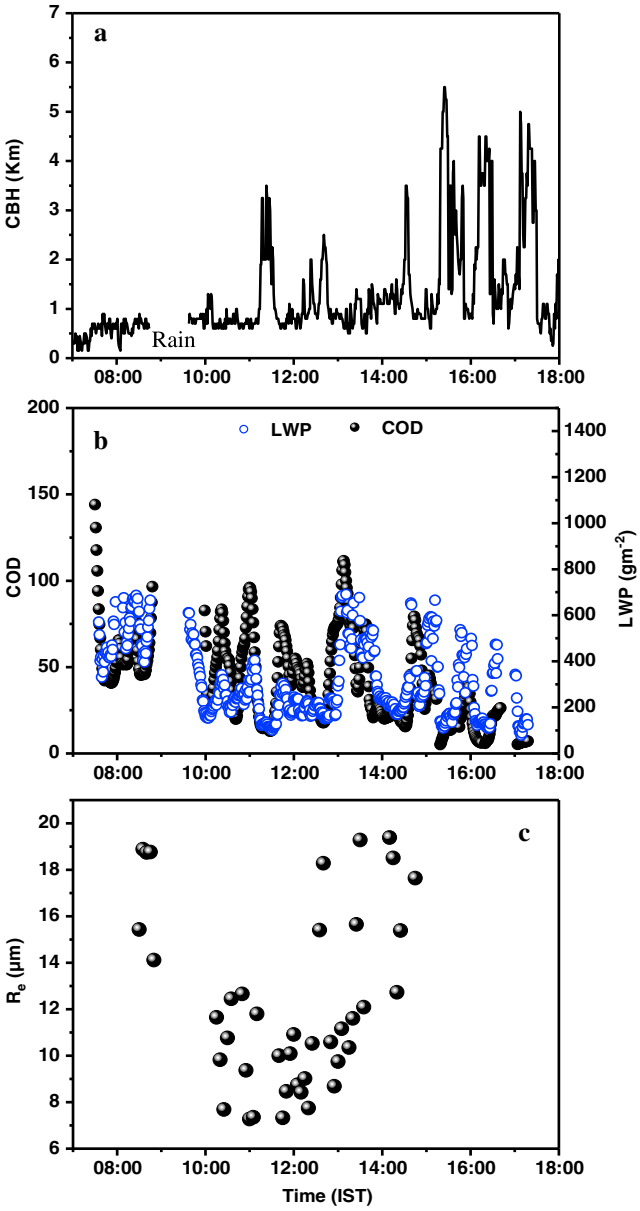

Figure 5. Time series of (a) cloud base height (CBH) and (b) cloud optical depth (COD) and liquid water path (LWP) and (c) droplet effective radius (R_e) for 25 August 2011.

shortwave radiometry [*Min et al.*, 2008]. On these days, the sky was mostly overcast throughout the day showing 100% cloud fraction with some periods of broken clouds.

1. Case 1 (22 August)
   The monsoon trough shifted toward the foothills of the Himalayas on 22 and 23 August. During this period, the central part of India received deficit amount of rainfall. Time series of CBH on 22 August is shown in Figure 4a. Over the observational site, the CBH varied from 0.5 to 1 km up to 08:00 h IST (Indian Standard Time), started to increase up to 11:00 h IST, and then decreased to 1 km toward noon time. It rained after 13:00 h IST. Later, the CBH again rose to 2 km. Figure 4b shows the time series of COD and LWP at 1 min time resolution. COD varied from 10 to 30, indicating that the clouds are not very thick. Two hours before rain, COD was only 10 and LWP was also less. Later with increase in LWP, COD also increased indicating the growth of cloud and evolution of precipitation which has been confirmed by the rainfall recorded after 13:00 h. Even though COD is derived from transmittance data, intrinsically, it is dependent upon LWP. During the time period 08:30 to 10:00 h IST, COD is more but LWP is low. This may be due to the presence of mixed phase clouds, as the CBH also lifted to 3 km and their tops might have extended beyond the freezing level. MFRSR retrieves total optical depth for both phases of clouds [see *Wang and Min,* 2008 for more details], while MWRP mainly detects liquid water of clouds and retrievals are unreliable during precipitating periods and ice cloud cases [*Illingworth et al.,* 2007]. This explains the poor correlation observed in the presence of mixed phase clouds. From 10:00 to 11:00 IST, the CBHs are even higher indicating mixed phase clouds, but COD is less compared to previous timings. In this case the cloud tops might not have extended much higher as before. On this day, LWP values were very low and COD values were also less comparatively. This might be due to less moisture incursion in a weak southwesterly flow, normally observed during weak monsoon conditions prevailing when the monsoon trough shifts to the north of its normal position.
2. Case 2 (25 August)
   During this period, the monsoon trough shifted to the south of its normal position and stayed almost more than 3 weeks at this position resulting in good rainfall activity over different parts of the country. On

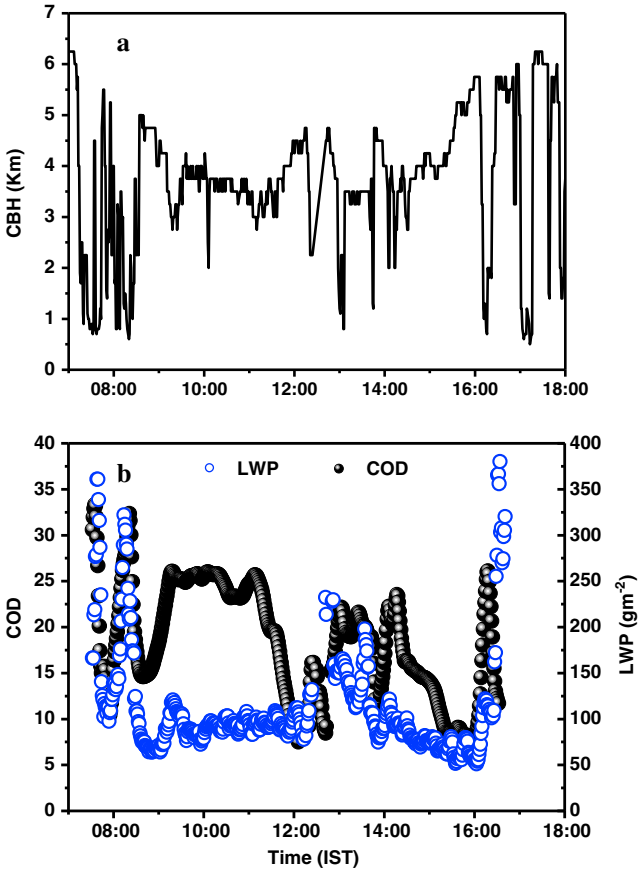

Figure 6. Time series of (a) cloud base height (CBH) and (b) cloud optical depth (COD) and liquid water path (LWP) for 12 October 2011.

25 August, convective clouds dominated during the entire day over the observational site and the cloud fraction was 100% for most of the time. From Figure 5a, it is noted that the CBH was very low and varied from 0.5 to 1 km with occasional lifting of the cloud base. From 09:00 h to 09:30 h IST, sparse spells of rain occurred. On this day, COD and LWP values were very high (Figure 5b) as compared to earlier case, indicating optically thick clouds with low CBHs. They showed high temporal variability due to continuous movement of clouds over the region. Drizzle occurred for a short period between 1500 h and 1515 h IST with very small droplets. After that, clouds were scattered. R_e retrievals for low CBHs, averaged for 5 min (Figure 5c), also showed high variability. Before the rain spell, between 09:00 h and 09:30 h IST, R_e crossed 12 μm (threshold for warm rain initiation) [*Kulkarni et al.*, 2012]. After rain it decreased to a minimum of about 7 μm and again crossed 12 μm. Though R_e is much higher than the threshold value between 14:00 and 15:00 h IST, it drizzled only for a short duration of 15 min. After noon time the CBHs increased and the height at which rain initiation takes place in the cloud also would have increased. As a result, the precipitation reaching the ground is reduced and only drizzle realized with smaller droplets.

3. Case 3 (12 October)
   During this period, northeast monsoon was set over south India and the airmass flow was from the east and northeast (as seen in Figure 2d). On this day, up to 08:30 h in the morning, there existed easterly flow up to midlevels, while after 08:30 h, only the lower level airmass was from the land (northeast) bringing in the continental pollutants. Over the site, homogeneous clouds were observed from the sky images. From Figure 6a, it is noted that the CBH was at about 1 km up to 08:30 h IST; later it varied in between 3 and 5 km. Most of the time, homogeneous middle level clouds were observed with almost 100% cloud fraction throughout the day. No rain was recorded and the clouds seem to be highly nonprecipitating. The time series of COD and LWP are shown in Figure 6b. The observed COD and LWP values were very small and showed similar variability except in the time period 09:30 to 11:30 h IST. During this period, the CBH increased to 3–3.5 km and remained homogeneous for nearly 2 h, where COD and LWP showed almost constant values of ~ 25 and ~ 100 gm^{-2}, respectively. At some time periods (12:30 h and 15:30 h IST), COD was less than 10 where the CBH was lifted above 4 km, indicating the presence of very thin clouds.

5.2. Statistics of Monsoon Cloud Properties

5.2.1. Variability of CF and CBH

The frequency of occurrence of cloud fraction (CF) and CBH from July to October over the observational site is shown in Figures 7a and 7b. Data are processed at every 5 min interval. One hundred percent CF with highest percentage of occurrence (55%) is observed in the month of August followed by July (30%), September (20%), and October (10%), as the availability of PWC is more in August as compared to other

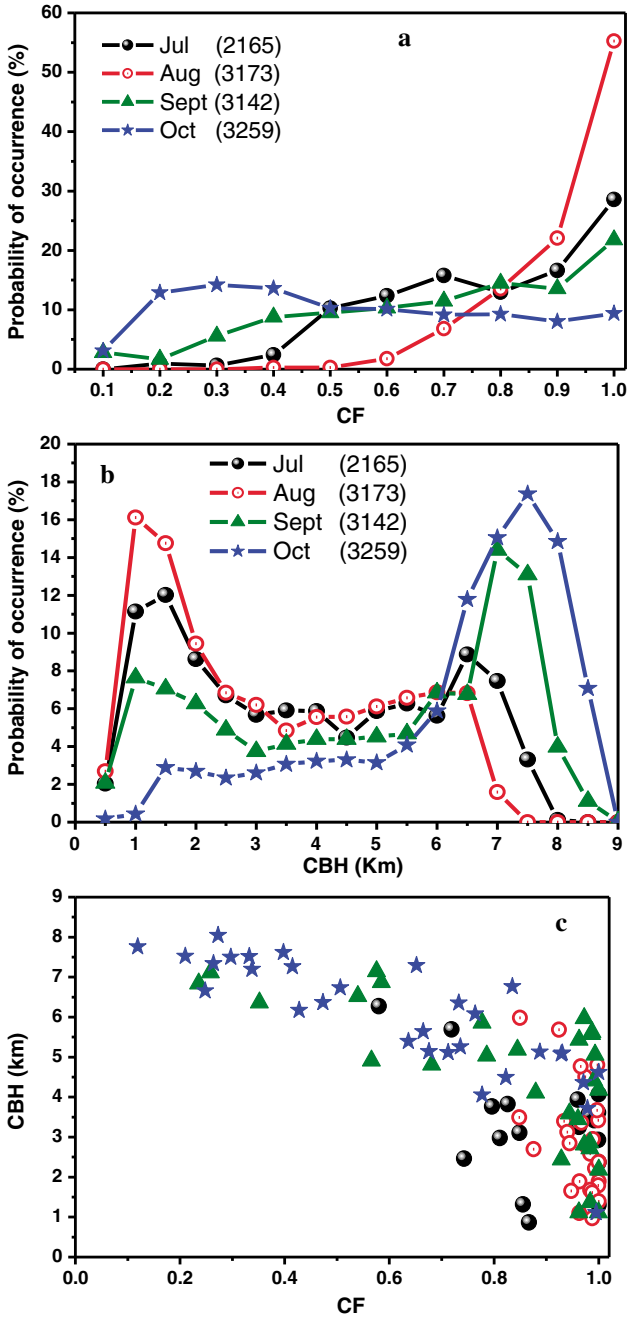

Figure 7. Ground-based retrievals of (a) CF and (b) CBH. The numbers in the bracket represent the number of data points used in the statistics. (c) Relationship between CF and CBH, where each data point represents daily average.

months (as seen in Figure 2). The occurrence of clouds with low CBHs 1–1.5 km is observed more in August followed by July, September, and October, as July and August are the peak monsoon months and low cloud bases are expected, while the occurrence of CBH $>$ 7 km is more in October followed by September. From September onward, withdrawal phase of monsoon starts and gradually moisture influx reduces over the peninsula, wind reversal takes place (as seen in Figures 2c and 2d), and clouds with higher bases are observed. Large variability in CBH is observed at $<$3 km and $>$6 km, while very less variability is observed between 3 and 6 km indicating the presence of midlevel clouds during all the months.

Figure 7c shows the relationship between the daily averages of CF and CBH. In all the months, lower CBH ($<$ 2 km) showed CF greater than 85%. On few days, higher CBHs also showed 100% CF. As the average height of the freezing level over this region varied from 5 to 5.5 km (Figure S1), it is noticed that during July and August, most of the time the cloud bases are well below the freezing level indicating the dominance of water phase clouds. In September, cloud bases are below as well as above the freezing level indicating the dominance of water phase clouds as well as mixed phase clouds. While in October, most of the time the cloud bases are above the freezing level indicating mixed phase or ice phase clouds and of convective origin.

5.2.2. Variability of LWP and COD

The monthly frequency distributions of LWP and COD for overcast and nonprecipitating clouds, processed at every 5 min interval, are shown in Figures 8a and 8b. LWP showed the maximum probability of occurrence at 100 gm^{-2} for the monsoon months, while October showed maximum at a lower value of 50 gm^{-2}. July and August also showed the second maximum at 150 gm^{-2}. Clouds with LWP $>$100 gm^{-2} are also observed but with less probability of occurrence. Clouds with LWP $<$ 100 gm^{-2} are usually considered to be optically thin water clouds [*Marchand et al.*, 2003]. Month-to-month variability in LWP is in concurrence with CF and CBH in those months. The frequency of occurrence of COD showed no wide variability from month to month. All the months showed maximum probability of occurrence at 20.

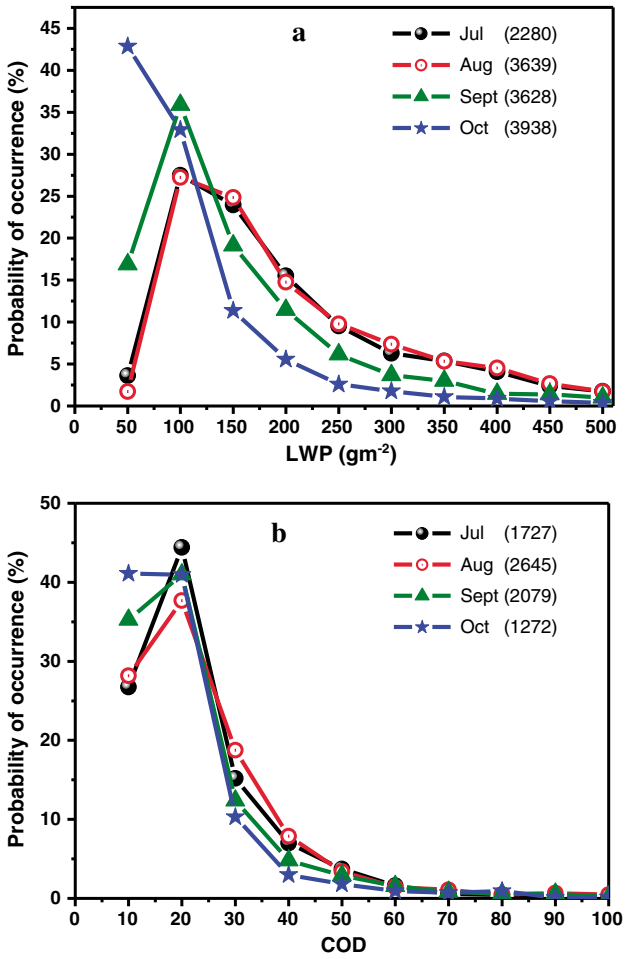

Figure 8. Ground-based retrievals of (a) LWP and (b) COD for overcast and nonprecipitating clouds. The numbers in the bracket represent the number of data points used in the statistics.

In Figure 9, daily averages for overcast conditions having at least 1 h continuous data are considered. Reasonably good correlation is observed between COD and LWP though they are derived from two different remote sensing techniques (Figure 9a). Occurrence of higher COD is found to be associated with higher LWP and vice versa. During July and August, daily average LWP varied up to 400 gm^{-2} with simultaneous COD variation of up to 35 and 55 in July and August, respectively. While during September and October, most of the population of LWP and COD values falls below 300 gm^{-2} and 40, respectively. Month-wise variability of LWP in association with CBH is depicted in Figure 9b. Higher LWPs with lower CBHs during peak monsoon months is due to the availability of more moisture from surface to midlevels. During September and October, CBHs are higher with lower LWPs due to lack of moisture and influx of continental airmass.

5.2.3. Variability of R_e

R_e retrieved from the combination of ground-based radiometers at a time resolution of 1 min is shown in Figure 10. In this analysis, apart from the criterion used for overcast sky, nonprecipitating clouds, and LWP between 20 and 700 gm^{-2}, another criterion used is CBH $<$ 2 km for July, August, and September months (as CBHs are very low in these months) and CBH $<$ 3 km for October month (as CBHs are higher than other months) to represent warm cloud. The monsoon months show nearly similar variability with maximum at 14–16 μm. This indicates that during monsoon there is influx of moisture from the southwesterly oceanic flow representing cleaner clouds, while the postmonsoon month shows entirely different feature from the other months. R_e shows a maximum at 12 μm and then falls and fluctuates thereafter. The probability of occurrence of clouds with R_e less than 12 μm is slightly higher in October as compared to other months. In this month, wind reversal takes place from southwesterly (maritime) to northwesterly/northeasterly (continental) (as seen in Figure 2) and dry airmass prevail over the region with less PWC and humidity which inhibit the cloud droplet growth. Also, the continental airmass laddened with aerosols might lead to the formation of polluted clouds having more number of smaller cloud droplets in the available liquid water content resulting in less R_e, indicating aerosol indirect effect. Occurrence of convective clouds with higher cloud bases is usually observed during this period. As a result, droplets grow much faster due to the presence of updrafts and reach the critical drop size of 12 μm. From in situ measurements over the Indian subcontinent, it is learnt that the critical R_e for warm rain initiation is between 10 and 12 μm in the polluted clouds and it is between 12 and 14 μm in cleaner monsoon clouds [*Kulkarni et al.*, 2012]. Though the statistics show the maximum R_e around 14–16 μm, the probability of occurrence is very less (10–12%) which might be the characteristic feature of the study region falling under the rain shadow belt.

5.2.4. Comparison With Aircraft Measurements

Airborne measurements were made from the base Hyderabad toward its southwestern sector as a part of CAIPEEX program. In the present study, one case observed on 16 September is considered, where the aircraft

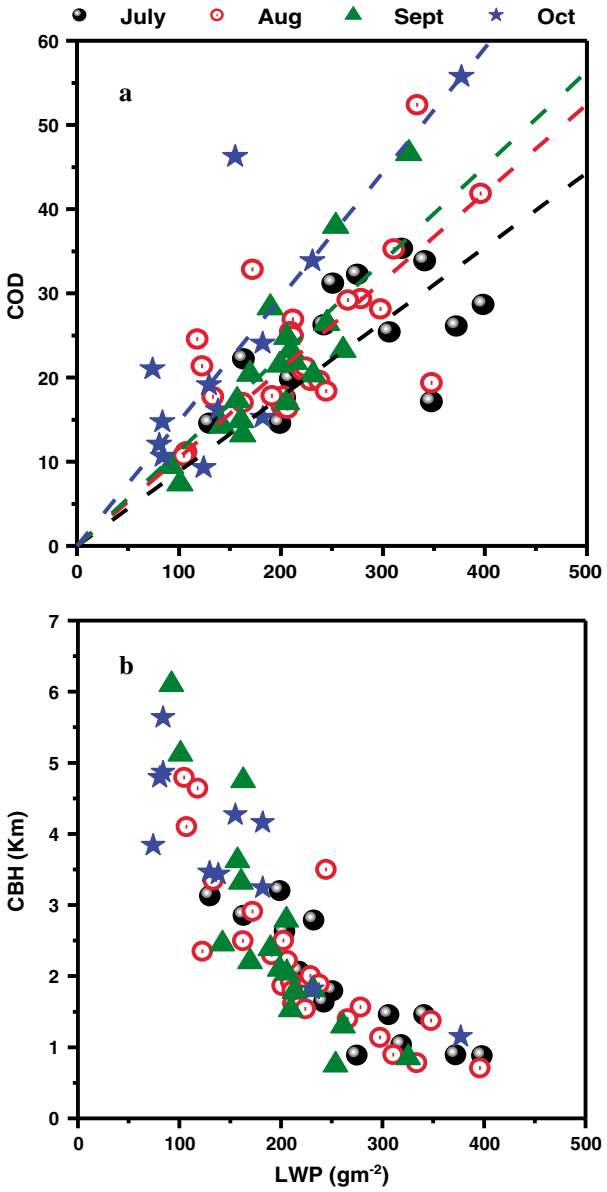

Figure 9. Relationship between the ground-based retrievals of (a) LWP and COD and (b) LWP and CBH. Each data point represents daily average.

profiled warm convective cumuli available toward east, 10 km away from the experimental site between 1330 h and 1530 h IST. Clouds were profiled vertically from the cloud top (3.8 km) to the cloud base. Figure 11 depicts the vertical distribution of R_e from FSSP. R_e increasing with height illustrates a growing cloud but not reaching the threshold for warm rain initiation [*Kulkarni et al.,* 2012]. Mean R_e from ground-based radiometers (12.0 ± 3.7 μm) and from aircraft (8.14 ± 1.4 μm) averaged for the flight duration is also depicted in the same figure. Ground-retrieved R_e is larger than aircraft-retrieved R_e. This difference might be due to different observational locations representing different cloud sampling volumes. It is interesting to note that R_e retrieved from different measurement techniques still fall within their standard deviations illustrating a fairly good agreement within the experimental constraints.

5.2.5. Comparison With MODIS

Intercomparison of ground-based and MODIS-Terra and MODIS-Aqua-derived COD, LWP and R_e over the observational site is shown in Figure 12. Care has been taken to match the temporal and spatial scales between the two measurements. One hour average of ground-based measurements has been considered centering at the time of MODIS overpass over the region to maximize the number of ground-based sample points and to minimize the number of satellite pixels [*Dong et al.*, 2008; *Liu et al.*, 2013]. MODIS products at 1 km resolution which falls within 2 km of the observational site were chosen. For this analysis, nonprecipitating warm cloud retrievals only are considered. During the four months of observational period, in total there were about 14 and 12 cases which were collocated with MODIS-Terra and MODIS-Aqua overpasses, respectively, and satisfying the above criterion. Intercomparisons with MODIS-Terra (overpass time 05:00 GMT, 10:30 IST) are shown in Figures 12a–12c. and MODIS-Aqua (over pass time 8:00 GMT, 13:30 IST) are shown in Figures 12d–12f. The horizontal bars represent the standard deviation of the ground retrievals made within 1 h centered around the satellite over pass time, and the vertical bars are the uncertainty in the MODIS mean retrieval. It is observed that on an average, MODIS-retrieved mean COD and LWP are underestimated, while mean R_e is overestimated as compared to ground retrievals. These results are similar to that reported over midlatitudes [*Dong et al.*, 2008; *Liu et al.*, 2013]. MODIS-Terra COD and LWP are underestimated by 12.8 and 195 gm^{-2}, respectively, and R_e overestimated by 0.33 μm, while MODIS-Aqua COD and LWP are underestimated by 11.8 and 233 gm^{-2}, respectively, and R_e overestimated by 1.58 μm. Liquid cloud droplets grow from cloud base to cloud top, as generally seen from in situ measurements [*Morwal et al.*,

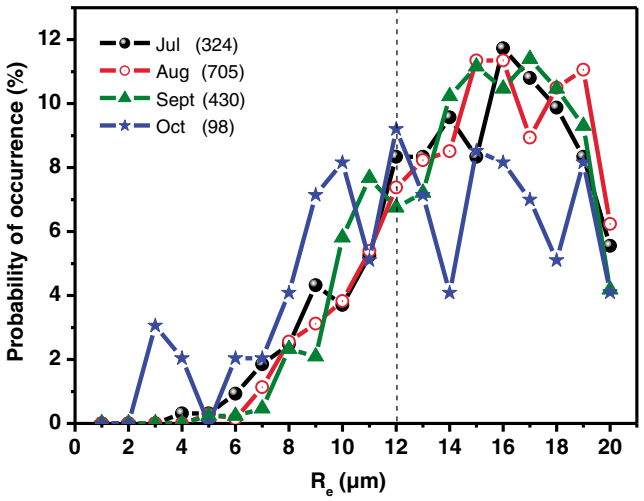

Figure 10. Ground-based radiometers derived cloud droplet effective radii (R_e) for overcast nonprecipitating clouds with CBH <2 km for July, August, and September months and CBH < 3 km for October month over Mahabubnagar. The numbers in the bracket represent the number of data points used in the statistics.

2012; *Min et al.*, 2012]. Satellite-retrieved R_e typically represents cloud droplets near the top of optically thick clouds [*Chang and Li*, 2003], while ground-retrieved R_e represents the layer mean cloud droplets [*Min et al.*, 2003]. This could explain why R_e from satellite-based retrievals is higher than ground-based retrievals.

Relative differences between the two techniques are estimated as [(MODIS-surface) / surface] × 100%). For MODIS-Terra, the relative differences are −65.6%, −77.0%, and 2.5% for COD, LWP, and R_e, respectively. For MODIS-Aqua, the relative differences are −56.5%, −72.4%, and 11.6% for COD, LWP, and R_e, respectively. More bias is observed between MWRP measured and MODIS-retrieved LWP compared to ground-retrieved and MODIS-retrieved COD and R_e. The observed biases are found to be more over the tropical region (the present study) as compared to midlatitudes reported so far, which needs further investigation.

The biases between the ground- and satellite-based retrievals are due to the information obtained from different levels within the cloud layer. For satellite-based retrievals, radiative contribution mainly comes from the upper portion of the cloud layer, while for ground-based retrievals, it comes from different levels within the cloud layer [*Min and Harrison*, 1996a, 1996b; *Chiu et al.*, 2012]. Satellite sensor looks at 1 km region where in cloud cover variability may not be homogeneous. Apart from this, mismatching in terms of the sampled cloud volume, viewing, and illumination angles of the satellite [*Min et al.*, 2004b; *Dong et al.*, 2008] also influence the comparison between the retrievals.

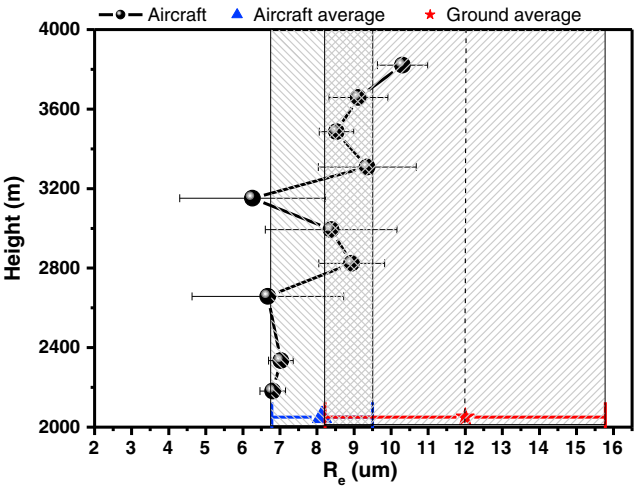

Figure 11. Vertical profile of aircraft-retrieved R_e. Also shown are simple averages of aircraft R_e and ground-retrieved R_e with standard deviation bars (SD). The shaded portions show the regions of SDs of ground- and aircraft-retrieved R_e.

6. Summary and Conclusions

The retrievals of cloud optical properties such as COD, LWP, and R_e from the ground-based radiometers over a rain shadow region in India, which experiences a complex and a wide variety of cloud types, is very challenging. Here an attempt is made for the first time to retrieve the monsoon cloud optical properties over Mahabubnagar in southern Indian peninsula.

Min and Harrison's [1996a, 1996b] retrieval algorithm is used to derive the monsoon cloud properties from solar irradiance measured by MFRSR and LWP measured by MWRP during July to October 2011. Over this region, low, medium, and high clouds with varying CBHs were observed during the

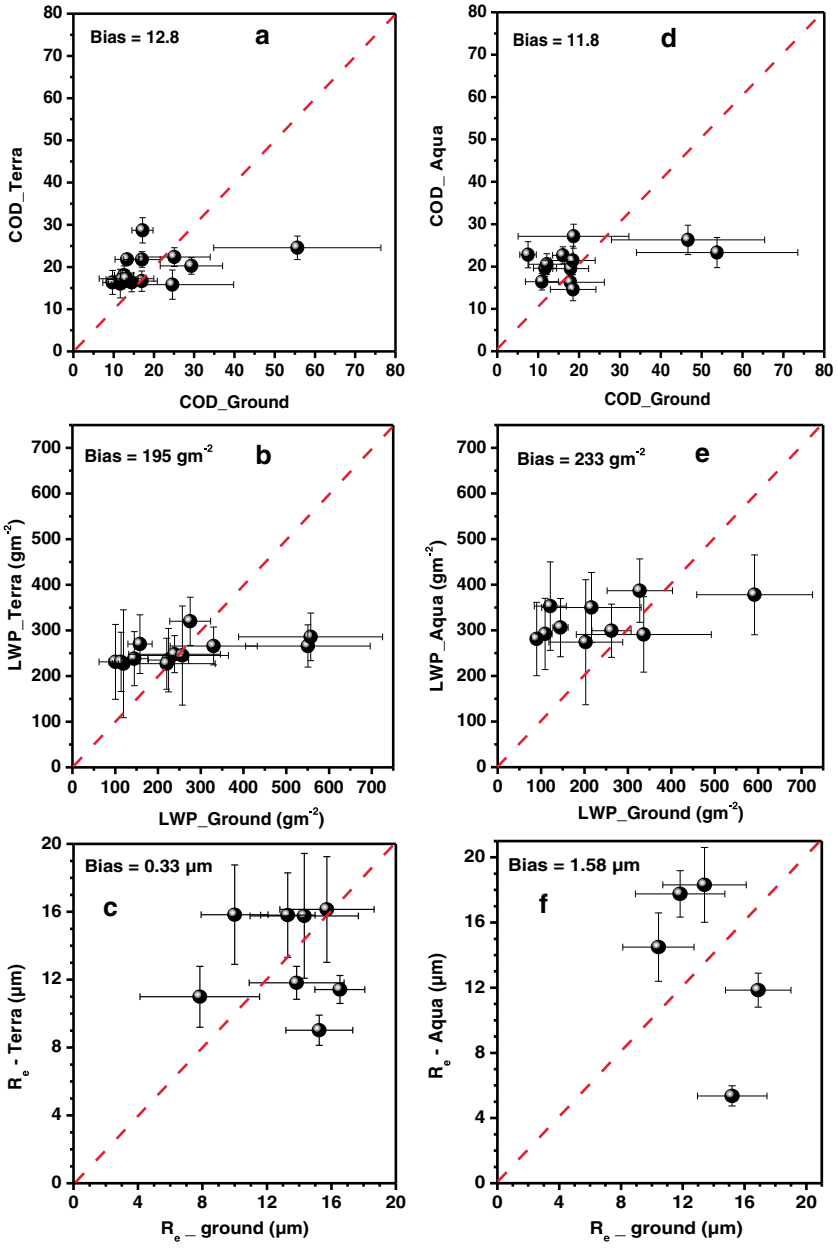

Figure 12. Comparison of retrievals from ground measurements and (left) MODIS-Terra and (right) MODIS-Aqua of COD, LWP, and R_e. The horizontal bars in each plot are the standard deviations of surface measurements during 1 h time window centered at the MODIS overpass time, and vertical bars represent the MODIS mean retrieval uncertainty.

observational period. COD and LWP retrieved from two independent measurements of MFRSR and MWRP showed reasonably good correlation for most of the time. However, during the presence of mixed phase clouds, the correlation weakened. Daily average LWP varied up to 400 gm^{-2} during the peak monsoon months of July and August with simultaneous COD variation of 35 (July) to 55 (August), while during monsoon withdrawal phase in September and postmonsoon in October, most of the population of LWP and COD values falls below 300 gm^{-2} and 40, respectively. Lower CODs and lower LWPs in September and October are associated with less moisture influx and higher CBHs.

During monsoon (July to September) and postmonsoon (October) months, the maximum probability of occurrence of COD is 20 under overcast conditions. During monsoon months the maximum probability of occurrence of LWP is 100 gm^{-2}, where most of the times the cloud bases are well below the freezing

level indicating the dominant presence of water clouds. While October showed maximum occurrence at a lower value of 50 gm^{-2}, where most of the times the cloud bases are above freezing level indicating the presence of mixed phase clouds.

R_e is retrieved from the ground radiometers under the criterion of overcast sky and warm cloud. From monsoon to postmonsoon transition, the maximum probability of occurrence of R_e varied from 14–16 μm to 12 μm, respectively. This indicates that during monsoon there is continuous influx of moisture from the southwesterly oceanic flow representing cleaner clouds. While during October, due to reversal in wind direction from marine to continental, there is influx of dry continental airmass with less water vapor content, which inhibit the droplet growth. Also, the dry airmass laddened with aerosols might lead to reduction in R_e in the available liquid water content, which is known as aerosol indirect effect. Though the monsoon statistics show the maximum R_e around 14–16 μm, the probability of occurrence is very less (10–12 %) which might be the characteristic feature of the study region falling under the rain shadow belt. Comparison with aircraft measurements show that R_e retrieved from different measurement techniques fall within their standard deviations illustrating a fairly good agreement within the experimental constraints.

Intercomparison of ground-based and MODIS-Terra and MODIS-Aqua-derived COD, LWP and R_e over the observational site for overcast and warm clouds indicates that on an average, MODIS-retrieved mean COD and LWP are underestimated, while mean R_e is overestimated as compared to ground retrievals. Based on 14 MODIS-Terra overpasses, relative to surface measurements, the mean biases are 12.8 (−65.6%), 195 gm^{-2} (−77.0%), and 0.33 μm (2.5%) for COD, LWP, and R_e, respectively, while the mean biases are 11.8 (−56.5%), 233 gm^{-2} (−72.4%), and 1.58 μm (11.6%) for COD, LWP and R_e, respectively, based on 12 MODIS-Aqua overpasses. The observed biases are found to be more over the tropical region (the present study) as compared to midlatitudes reported so far.

The continuous ground-based retrievals are much useful to understand the temporal and diurnal variability of cloud properties over a region, which cannot be achieved with satellite and in situ measurements.

Acknowledgments

The authors wish to thank Prof. B. N. Goswami, Director, IITM, for his constant encouragement and support. Thanks are also due to the team members of CAIPEEX and ground observational campaign (IGOC). This project is funded by the Ministry of Earth Sciences (MoES), Government of India. Authors also wish to thank MODIS Atmospheres Team. Data may be shared through possible collaboration. We also thank the anonymous reviewers for their constructive suggestions in improving the manuscript.

References

Barker, H. W., T. J. Curtis, E. Leontieva, and K. Stamnes (1998), Optical depth of overcast cloud across Canada: Estimates based on surface pyranometer and satellite measurements, *J. Clim.*, *11*, 2980–2994.

Bevington, P. R. (1969), *Data Reduction and Error Analysis for the Physical Sciences*, McGraw-Hill, New York.

Brenguier, J.-L., H. Pawlowska, L. Schuller, R. Preusker, J. Fischer, and Y. Fouquart (2000), Radiative properties of boundary layer clouds: Droplet effective radius versus number concentration, *J. Atmos. Sci.*, *57*, 803–821, doi:10.1175/1520-0469.

Chang, F.-L., and Z. Li (2003), Retrieving vertical profiles of water-cloud droplet effective radius: Algorithm modification and preliminary application, *J. Geophys. Res.*, *108*(D24), doi:10.1029/2003JD003906.

Chiu, J. C., A. Marshak, C.-H. Huang, T. Várnai, R. J. Hogan, D. M. Giles, B. N. Holben, E. J. O'Connor, Y. Knyazikhin, and W. J. Wiscombe (2012), Cloud droplet size and liquid water path retrievals from zenith radiance measurements: examples from the Atmospheric Radiation Measurement Program and the Aerosol Robotic Network, *Atmos. Chem. Phys.*, *12*, 10,313–10,329, doi:10.5194/acp-12-10313-2012.

Christensen, M. W., and G. L. Stephens (2011), Microphysical and macrophysical responses of marine stratocumulus polluted by underlying ships: Evidence of cloud deepening, *J. Geophys. Res.*, *116*, D03201, doi:10.1029/2010JD014638.

Das, P. K. (1995), *The Monsoons*, 3rd ed., National Book Trust, India, New Delhi.

Dong, X., T. P. Ackerman, E. E. Clothiaux, P. Pilewskie, and Y. Han (1997), Microphysical and radiative properties of boundary layer stratiform clouds deduced from ground-based measurements, *J. Geophys. Res.*, *102*, 23,829–23,843.

Dong, X., P. Minnis, P. Ackerman, G. G. Mace, N. Long, and C. Liljegren (2000), A 25-month database of stratus cloud properties generated from ground-based measurements at the Atmospheric Radiation Measurement Southern Great, *J. Geophys. Res.*, *105*, 4529–4537.

Dong, X., P. Minnis, B. Xi, S. Sun-Mack, and Y. Chen (2008), Comparison of CERES-MODIS stratus cloud properties with ground-based measurements at the DOE ARM Southern Great Plains site, *J. Geophys. Res.*, *113*, D03204, doi:10.1029/2007JD008438.

Feingold, G., R. Furrer, P. Pilewskie, L. A. Remer, Q. L. Min, and H. Jonson (2006), Aerosol indirect effect studies at Southern Great Plains during the May 2003 intensive operations period, *J. Geophys. Res.*, *111*, D05S14, doi:10.1029/2004JD005648.

Harrison, L. C., and J. Michalsky (1994), Objective algorithms for the retrieval of optical depths from ground-based measurements, *Appl. Opt.*, *33*, 5126–5132, doi:10.1364/AO.33.005126.

Harrison, L. C., J. Michalsky, and J. Berndt (1994), Automated multifilter rotating shadow-band radiometer: An instrument for optical depth and radiation measurements, *Appl. Opt.*, *33*, 5118–5125.

Illingworth, A. J., et al. (2007), Cloudnet: Continuous evaluation of cloud profiles in seven operational models using ground-based observations, *Bull. Am. Meteorol. Soc.*, *88*, 883–898, doi:10.1175/BAMS-88-6-883.

Kalnay, E., et al. (1996), The NCEP/NCAR 40-year reanalysis project, *Bull. Am. Meteorol. Soc.*, *77*, 437–471.

Kikuchi, N., T. Nakajima, H. Kumagai, H. Kuroiwa, A. Kamei, R. Nakamura, and T. Y. Nakajima (2006), Cloud optical thickness and effective particle radius derived from transmitted solar radiation measurements: Comparison with cloud radar observations, *J. Geophys. Res.*, *111*, D07205, doi:10.1029/2005JD006363.

Kim, B.-G., S. E. Schwartz, M. A. Miller, and Q. L. Min (2003), Effective radius of cloud droplets by ground-based remote sensing: Relationship to aerosol, *J. Geophys. Res.*, *108*(D23), 4740, doi:10.1029/2003JD003721.

Konwar, M., R. S. Maheskumar, J. R. Kulkarni, E. Freud, B. N. Goswami, and D. Rosenfeld (2010), Suppression of warm rain by aerosols in rain-shadow areas of India, *Atmos. Chem. Phys. Discuss.*, *10*, 17,009–17,027.
Konwar, M., R. S. Maheskumar, J. R. Kulkarni, E. Freud, B. N. Goswami, and D. Rosenfeld (2012), Aerosol control on depth of warm rain in convective clouds, *J. Geophys. Res.*, *117*, D13204, doi:10.1029/2012JD017585.
Kubar, T. L., D. L. Hartmann, and R. Wood (2009), Understanding the importance of microphysics and macrophysics for warm rain in marine low clouds. Part I: Satellite observations, *J. Atmos. Sci.*, *66*, 2953–2972, doi:10.1175/2009JAS3071.1.
Kulkarni, J. R., et al. (2012), The Cloud Aerosol Interactions and Precipitation Enhancement Experiment (CAIPEEX): Overview and preliminary results, *Curr. Sci.*, *102*, 413–425.
Leontieva, E., and K. Stamnes (1996), Remote sensing of cloud optical properties from ground-based measurements of transmittance: A feasibility case, *J. Appl. Meteorol.*, *35*, 2011–2022, doi:10.1175/1520-0450.
Liao, L., and K. Sassen (1994), Investigation of relationships between Ka band radar reflectivity and ice and liquid water contents, *Atmos. Res.*, *34*, 231–248.
Liljegren, J. C., E. E. Clothiaux, G. G. Mace, S. Kato, and X. Q. Dong (2001), A new retrieval for cloud liquid water path using a ground-based microwave radiometer and measurements of cloud temperature, *J. Geophys. Res.*, *106*, 14,485–14,500.
Liu, J., Z. Li, Y. Zheng, J. C. Chiu, F. Zhao, M. Cadeddu, F. Weng, and M. Cribb (2013), Cloud optical and microphysical properties derived from ground-based and satellite sensors over a site in the Yangtze Delta region, *J. Geophys. Res. Atmos.*, *118*, 9141–9152, doi:10.1002/jgrd.50648.
Madhavan, B. L., Y. He, Y. Wu, B. Gross, F. Moshary, and S. Ahmed (2012), Development of a ground based remote sensing approach for direct evaluation of aerosol-cloud interaction, *Atmosphere*, *3*, 468–494, doi:10.3390/atmos3040468.
Marchand, R., T. Ackerman, E. R. Westwater, S. A. Clough, K. Cady-Pereira, and J. C. Liljegren (2003), An assessment of microwave absorption models and retrievals of cloud liquid water using clear-sky data, *J. Geophys. Res.*, *108*(D24), 4773, doi:10.1029/2003JD003843.
Matamoros, S., J.-A. González, and J. Calbo (2011), A simple method to retrieve cloud properties from atmospheric transmittance and liquid water column measurements, *J. Appl. Meteorol. Climatol.*, *50*, 283–295, doi:10.1175/2010JAMC2394.1.
McBride, P. J., K. S. Schmidt, P. Pilewskie, A. S. Kittelman, and D. E. Wolfe (2011), A spectral method for retrieving cloud optical thickness and effective radius from surface-based transmittance measurements, *Atmos. Chem. Phys.*, *11*, 7235–7252, doi:10.5194/acp-11-7235-2011.
Menzel, W. P., and M. R. A. Frey (2013), Cloud top properties and cloud phase algorithm theoretical basis document. Collection 006 update.
Min, Q.-L., and M. Duan (2005), Simultaneously retrieving cloud optical depth and effective radius for optically thin clouds, *J. Geophys. Res.*, *110*, D21201, doi:10.1029/2005JD006136.
Min, Q.-L., and L. C. Harrison (1996a), Cloud properties derived from surface MFRSR measurements and comparison with GOES results at the ARM SGP site, *Geophys. Res. Lett.*, *23*, 1641–1644, doi:10.1029/96GL01488.
Min, Q.-L., and L. C. Harrison (1996b), An adjoint formulation of the radiative transfer method, *J. Geophys. Res.*, *101*, 1635–1640.
Min, Q.-L., M. Duan, and R. Marchand (2003), Validation of surface retrieved cloud optical properties with in situ measurements at the Atmospheric Radiation Measurement Program (ARM) South Great Plains site, *J. Geophys. Res.*, *108*(D17), 4547, doi:10.1029/2003JD003385.
Min, Q.-L., E. Joseph, and M. Duan (2004a), Retrievals of thin cloud optical depth from a multifilter rotating shadowband radiometer, *J. Geophys. Res.*, *109*, D02201, doi:10.1029/2003JD003964.
Min, Q.-L., P. Minnis, and M. Khaiyer (2004b), Comparison of cirrus optical depths derived from GOES 8 and surface measurements, *J. Geophys. Res.*, *109*, D15207, doi:10.1029/2003JD004390.
Min, Q.-L., T. Wang, C. N. Long, and M. Duan (2008), Estimating fractional sky cover from spectral measurements, *J. Geophys. Res.*, *113*, D20208, doi:10.1029/2008JD010278.
Min, Q., E. Joseph, Y. Lin, L. Min, B. Yin, P. H. Daum, L. I. Kleinman, J. Wang, and Y.-N. Lee (2012), Validation of MODIS cloud microphysical properties with in situ measurements over the Southeast Pacific, *Atmos. Chem. Phys. Discuss.*, *12*(1), 1419–1449, doi:10.5194/acpd-12-1419-2012.
Morwal, S. B., R. S. Maheskumar, B. Padma Kumari, J. R. Kulkarni, and B. N. Goswami (2012), Cloud microphysical properties over Indian monsoon regions during CAIPEEX-2009, *J. Atmos. Sol. Terr. Phys.*, *81–82*, 76–85.
Norris, J. R., and M. Wild (2007), Trends in aerosol radiative effects over Europe inferred from observed cloud cover, solar "dimming," and solar "brightening", *J. Geophys. Res.*, *112*, D08214, doi:10.1029/2006JD007794.
Padma Kumari, B., and B. N. Goswami (2010), Seminal role of clouds on solar dimming over the Indian monsoon region, *Geophys. Res. Lett.*, *37*, L06703, doi:10.1029/2009GL042133.
Pandithurai, G., S. Dipu, T. V. Prabha, R. S. Maheskumar, J. R. Kulkarni, and B. N. Goswami (2012), Aerosol effect on droplet spectral dispersion in warm continental cumuli, *J. Geophys. Res.*, *117*, D16202, doi:10.1029/2011JD016532.
Pawlowska, H., W. W. Grabowski, and J.-L. Brenguier (2006), Observations of the width of cloud droplet spectra in stratocumulus, *Geophys. Res. Lett.*, *33*, L19810, doi:10.1029/2006GL026841.
Rao, Y. P. (1976), The southwest monsoon, India Meteorological Department.
Roebeling, R. A., A. J. Feijt, and P. Stammes (2006), Cloud property retrievals for climate monitoring: Implications of differences between Spinning Enhanced Visible and Infrared Imager (SEVIRI) on METEOSAT-8 and Advanced Very High Resolution Radiometer (AVHRR) on NOAA-17, *J. Geophys. Res.*, *111*, D20210, doi:10.1029/2005JD006990.
Slingo, A., S. Nicholls, and J. Schmetz (1982), Aircraft observation of marine stratocumulus during JASIN, *Q. J. R. Meteorol. Soc.*, *108*, 833–856.
Stamnes, K., S.-C. Tsay, W. Wiscombe, and K. Jayaweera (1988), Numerically stable algorithm for discrete-ordinate-method radiative-transfer in multiple-scattering and emitting layered media, *Appl. Opt.*, *27*, 2502–2509.
Stephens, G. L. (1978a), Radiation profiles in extended water clouds. I: Theory, *J. Atmos. Sci.*, *35*, 2111–2122, doi:10.1175/1520-0469.
Stephens, G. L. (1978b), Radiative properties of extended water clouds. II: Parameterization schemes, *J. Atmos. Sci.*, *35*, 2123–2132.
Wang, T., and Q. Min (2008), Retrieving optical depths of optically thin and mixed-phase clouds from MFRSR measurements, *J. Geophys. Res.*, *113*, D19203, doi:10.1029/2008JD009958.
Wang, Z., K. Sassen, D. N. Whiteman, and B. B. Demoz (2004), Studying altocumulus with ice virga using ground-based active and passive remote sensors, *J. Appl. Meteorol.*, *43*, 449–460.